Reliability Engineering and System Safety 182 (2019) 166–178

Contents lists available at ScienceDirect

Reliability Engineering and System Safety

journal homepage: www.elsevier.com/locate/ress

Battery health management for small-size rotary-wing electric unmanned aerial vehicles: An efficient approach for constrained computing platforms☆

G. Sierra*[,a], M. Orchard*[,a], K. Goebel[b,c], C. Kulkarni[d]

[a] Department of Electrical Engineering, University of Chile, Santiago, Chile
[b] NASA Ames Research Center, Moffett Field, CA 94035, USA
[c] Division of Operation and Maintenance Engineering, Luleå University of Technology, Luleå, Sweden
[d] SGT Inc., NASA Ames Research Center, Moffett Field, CA 94035, USA

ARTICLE INFO

Keywords:
Multirotor unmanned aerial vehicles
Li–Po battery end-of-discharge
Bayesian parameter estimation
Model-based prognostics
Efficient on-board prognostics

ABSTRACT

This article presents a holistic framework for the design, implementation and experimental validation of Battery Management Systems (BMS) in rotatory-wing Unmanned Aerial Vehicles (UAVs) that allows to accurately (i) estimate the State of Charge (SOC), and (ii) predict the End of Discharge (EOD) time of lithium-polymer batteries in small-size multirotors by using a model-based prognosis architecture that is efficient and feasible to implement in low-cost hardware. The proposed framework includes a simplified battery model that incorporates the electric load dependence, temperature dependence and SOC dependence by using the concept of Artificial Evolution to estimate some of its parameters, along with a novel Outer Feedback Correction Loop (OFCL) during the estimation stage which adjusts the variance of the process noise to diminish bias in Bayesian state estimation and helps to compensate problems associated with incorrect initial conditions in a non-observable dynamic system. Also, it provides an aerodynamic-based characterization of future power consumption profiles. A quadrotor has been used as validation platform. The results of this work will allow making decisions about the flight plan and having enough confidence in those decisions so that the mission objectives can be optimally achieved.

1. Introduction

UAVs have received much attention in recent years due to their wide range of military and civilian applications. Fixed-wing UAVs and rotary-wing UAVs are being used for surveillance, reconnaissance, mapping, cartography, border patrol, inspection, homeland security, search and rescue, fire detection, agricultural imaging, traffic monitoring, to name just a few application domains. Multicopters (a type of rotary-wing aircraft) have recently emerged as the platform of choice for a variety of uses. They can hover in place and take off and land vertically, unlike their fixed-wing counterparts [1]. In general, they are highly maneuverable and enable safe and low-cost experimentation in mapping, navigation, and control algorithms in three dimensions.

UAVs are ideally suited for long endurance applications and the flight endurance is in direct relationship to the total weight of the craft. Therefore, Lithium Polymer (Li–Po) batteries in electric UAVs are usually used as power source on account of their high density energy [2]. Nevertheless, electric UAVs experience problems and risks associated with the use of batteries as primary power source, such as temperature dependence, electric load dependence or aging dependence, and flight times are generally short [3].

The intensive use of Li–Po batteries in the electric vehicle industry has popularized the concept of Battery Management Systems (BMS). These systems are mainly aimed at using in a better way the energy stored in the batteries and provide real-time diagnosis information for the benefit of craft operator. To accomplish these tasks, BMS must use information about the battery's SOC and its Remaining Useful Life (RUL) [4]. The knowledge of these state variables is not only necessary to verify if the mission goal(s) can be accomplished but also important to aid in online decision-making activities such as fault mitigation and mission replanning.

SOC estimation and prognostic strategies are fundamental for the

☆ This work was supported in part by CONICYT under scholarship CONICYT-PCHA/Doctorado Nacional/2014-63140178, and in part by FONDECYT Chile Grant Nr. 1170044, and the Advanced Center for Electrical and Electronic Engineering, AC3E, Basal Project FB0008, CONICYT. Also, the authors want to thank project CONICYT PIA ACT1405

* Corresponding authors.
E-mail addresses: gina.sierra@ing.uchile.cl (G. Sierra), morchard@ing.uchile.cl (M. Orchard), kai.goebel@nasa.gov (K. Goebel), chetan.s.kulkarni@nasa.gov (C. Kulkarni).

https://doi.org/10.1016/j.ress.2018.04.030
Received 5 February 2018; Received in revised form 4 April 2018; Accepted 29 April 2018
Available online 18 May 2018

characterization of the EOD time. However, as in many other state estimation problems, the SOC is not observable, namely, it can not be directly measured and it has to be inferred from indirect but partially correlated measurements (e.g., the battery voltage, discharge current, or temperature) [4]. Because real value of SOC is not known with complete certainty, battery-powered electric UAVs suffer from uncertainties in estimating the remaining charge. Therefore most flight plans are highly conservative in nature, which means flight times are even shorter than what the battery capacity could support.

The development of BMS for battery-powered electric UAVs has focused on Bayesian-based methods [5–10] because they have provided decent results in estimation and prognosis problems. Among these methods are those based on Extended Kalman Filter (EKF) [11–13], Unscented Kalman Filter (UKF) [14–16], and Particle Filter (PF) [4,17,18]. Unlike other methods, Bayesian-based methods can adjust the SOC in real time for different load conditions [19] and they are able to assess the estimate's confidence by a Probability Density Function (PDF) [20]. Using the concept of *artificial evolution* in conjunction with Bayesian methods provides the mechanism for generating new parameter (e.g., the battery internal resistance) values at each time step by adding additional random disturbances to sampled state vectors, which has proved to be efficient because it incorporates the effect of environmental factors (e.g., temperature, or battery degradation and age). This concept is implemented by extending the dimension of the state vector of the system model [21,22]. For applications with a longer prediction horizon, a framework based on the combination of partial least squares (PLS) and Takagi-Sugeno (TS) fuzzy systems have been recently reported in [23] to produce real forecast models with a longer prediction horizon which would allow predicting voltage of batteries in a few hours based on current process values trends.

To use Bayesian estimation methods, the relationship between SOC and other measurable units, such as voltage, current or temperature, should be first established. Namely, a battery model as a function of SOC should be used, where usually the current is considered as an input. Although several battery state models have been reported with different levels of granularity and abstraction, they are typically complex and need to identify several parameters which is impractical in real time applications. Performance show that higher granularity and lower levels of abstraction might generally give more accurate predictions, but they also result in larger parameter sets which may not have good convergence properties if included in the state vector [5].

In [24], a model for battery prognostics based on the underlying physics is presented. Using equations based on electrochemistry, they developed a model that is both accurate and efficient, unlike previous electrochemistry-based models which are often computationally inefficient. As a result, prognostics results for EOD prediction were shown to be very accurate, with the uncertainty associated with the model remaining very small. Nevertheless, this approach requires a large number of parameters (27 parameters) to be estimated off-line. These could be difficult to optimally find considering the constraints imposed by the model. In [4], an equivalent circuit battery model is introduced, namely, an empirical model that allows the implementation of Bayesian filtering methods that efficiently and effectively estimate the SOC in real-time and only requires the estimation off-line of 7 parameters. However, its parameterization for the Open Circuit Voltage (OCV) curve is insufficient for batteries of more than one cell.

In addition, a proper future load profile characterization leads to End of Discharge (EOD) predictions that are more accurate and more stable as well [7]. Future load profile can be inferred from the flight plan, namely, length and speed of each flight phase, for example, climb, hover, forward flight, etc. The other major factors that affect performance and power consumption are density altitude (air density relative to altitude, pressure and temperature), weight, and, wind direction and velocity [25]. As the air becomes thinner with altitude and heat, this greatly decreases the propeller's ability to generate lift.

The future load profile characterization has been addressed by establishing a mean current for each flight maneuver based on either historical data of typical flights [5] or aerodynamic models [8]. Then, a PDF is defined around the current mean in order to characterize the uncertainty associated with unmodeled phenomena (e.g., temperature) [6,7]. However, while aforementioned studies are aimed at fixed-wing aircraft (with the exception of de Souza Candido et al. [9] which is aimed at rotary-wing aircraft, although it is limited to numerical simulations and hover flight) little work has been done regarding to BMS for rotary-wing UAVs. Because rotary-wing and fixed-wing aerodynamics are different, their performances and power consumptions in each flight maneuver are different as well. Therefore, BMS for rotary-wing UAVs must consider a characterization of the power consumption in rotary-wing aircraft in order to properly define the future load profiles used in prognostic.

UAVs usually have weight, size and cost constraints. Therefore, there is a need to accurately (i) estimate the State of Charge (SOC), and (ii) predict the End of Discharge (EOD) time of Li–Po batteries in small-size multirotors that can operate in constrained environments.

To reduce computational resources without losing accuracy, this paper proposes a simplified equivalent circuit battery model that takes advantage of artificial evolution to estimate some of its parameters, along with an Outer Feedback Correction Loop (OFCL) during the estimation stage which adjusts the variance of the process noise to diminish the bias in Bayesian state estimation. In addition, an aerodynamic-based model of the power required is proposed instead of using a large amount of flight data or flight simulations to define future power consumption profiles. A small quadrotor is used as validation platform.

This paper is organized as follows. Section 2 describes the model-based prognostics architecture. Section 3 presents the suggested state-space model for batteries and its validation. Section 4 describes a novel OFCL. Section 5 deals with the problem of characterizing future power profiles using an aerodynamic-based model. In Section 6, the proposed solution is evaluated in terms of effectiveness and efficiency, and the results are presented and discussed. Section 7 ends with conclusions.

2. Prognostics architecture

We adopt a model-based prognostics architecture [26] where there is a system being monitored, and one develops a model describing how the system evolves in time in response to its inputs [27]. We assume the system model may be generally defined as

$$x(k+1) = f(k, x(k), \theta(k), u(k), v(k)), \tag{1}$$

$$y(k) = h(k, x(k), \theta(k), u(k), n(k)), \tag{2}$$

where k is the discrete time variable, $x(k) \in \mathbb{R}^{n_x}$ is the state vector, $\theta(k) \in \mathbb{R}^{n_\theta}$ is the unknown parameter vector, $u(k) \in \mathbb{R}^{n_u}$ is the input vector, $v(k) \in \mathbb{R}^{n_v}$ is the process noise vector, f is the state equation, $y(k) \in \mathbb{R}^{n_y}$ is the output vector, is the measurement noise vector, and h is the output equation.

In prognostics, we are interested in predicting the occurrence of some event E that is defined with respect to the states, parameters, and inputs of the system. We define the event as the earliest instant that some event threshold T_E is reached. For batteries, we are interested in predicting the EOD, defined by a voltage threshold V_{EOD}. In this case, T_E is defined by $V < V_{EOD}$, that is, when the battery voltage is less than the cutoff voltage, EOD is reached.

That model is used as the basis of two sequential problems, (*i*) the estimation problem, which requires determining a joint state-parameter estimate $p(x(k),\theta(k)|y(k_0{:}k))$ based on the history of observations up to time k, $y(k_0{:}k)$, and (*ii*) the prediction problem, which determines at k_P, using $p(x(k),\theta(k)|y(k_0{:}k))$, a probability distribution $p(k_E(k_P)|y(k_0{:}k_P))$. The distribution for Δk_E can be computed from $p(k_E(k_P)|y(k_0{:}k_P))$ by subtracting k_P. The prognostics architecture is shown in Fig. 1. In discrete time k, the system is provided with inputs u_k and provides

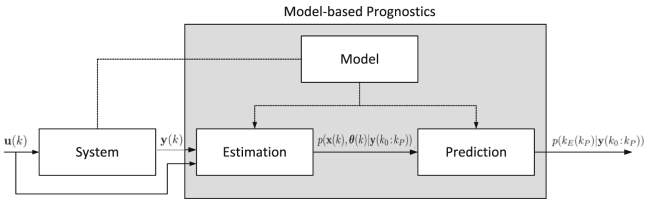

Fig. 1. Model-based prognostics conceptual architecture.

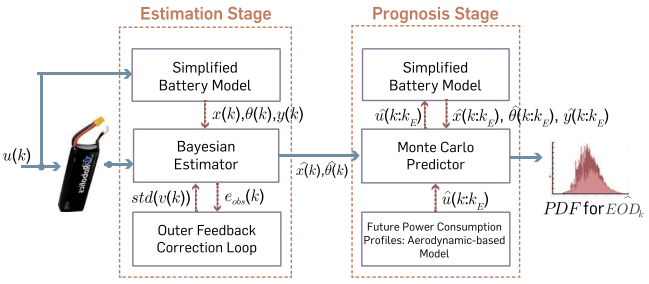

Fig. 2. Framework outline

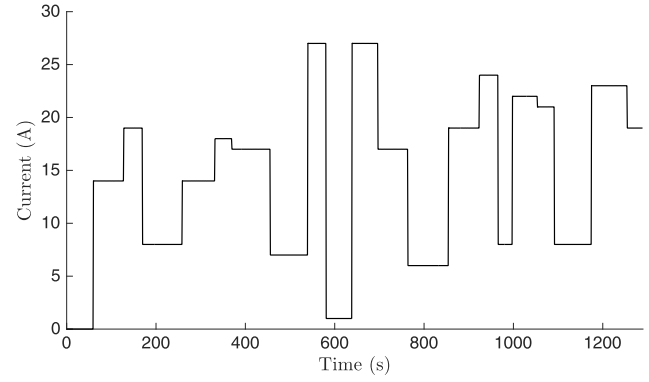

(a) Current

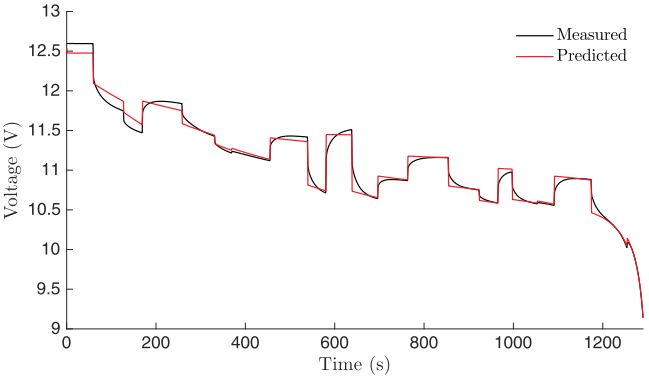

(b) Measured and predicted variable loading discharge curves.

Fig. 3. Off-line estimation of the model parameters. Curve fitting for a variable current.

measured outputs y_k. The estimation module uses this information, along with the system model, to compute an estimate $p(x(k),\theta(k)|y(k_0{:}k))$. The prediction module uses the joint state-parameter distribution and the system model, along with hypothesized future inputs, to compute the probability distribution $p(k_E(k_P)|y(k_0{:}k_P))$ at given prediction times k_P.

In addition, this study includes an OFCL during the estimation stage and also provides an aerodynamic-based characterization of the future

Table 1
Equivalent circuit model parameters for a 3S 5100 mAh Li–Po battery.

Parameter	Symbol	Value
Battery model parameter	β	8.482
Battery model parameter	γ	3.355
Battery model parameter	λ	0.046
Battery model parameter	μ	2.759
Battery model parameter	v_L	11.148
Initial total energy (J)	$E_{crit}(k_0)$	202, 426.858
Initial Internal resistance (Ω)	$R_{int}(k_0)$	0.027
Sample time (s)	Δt	1
Process noise covariance matrix	R_{ww}	$\begin{bmatrix} 1.2{\cdot}10^{-7} & 0 & 0 \\ 0 & 1.163{\cdot}10^{-7} & 0 \\ 0 & 0 & 176.3 \end{bmatrix}$
Observation noise covariance	R_{vv}	$1.\ 1^{-3}$

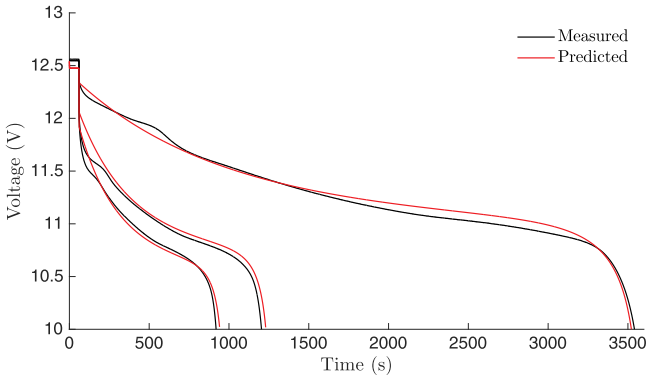

Fig. 4. Model validation. Measured and predicted 1C, 3C and 4C rate discharge curves.

if $t > t_{min}$ **then**
  $e_{acum} = e_{acum} + |e_{obs}|$
  if $e_{acum} \leq e_{thr}$ **then**
    $std(w_i(t)) = max(p_i \cdot std(w_i(t)), std_i)$
  else
    $e_{acum} = 0$
    $std(w_i(t)) = q_i \cdot std(w_i(t))$
  end if
end if

Algorithm 1. Outer feedback correction loop (OFCL) by Tampier et al. [29].

$e_{avg} = e_{avg} \cdot \left(1 - \frac{1}{2^n}\right) + |e_{obs}| \cdot \frac{1}{2^n}$
if $e_{avg} \leq e_{thr}$ **then**
  $std(w_i(k)) = max(p_i \cdot std(w_i(k)), std_{min_i})$
else
  $std(w_i(k)) = min(q_i \cdot std(w_i(k)), std_{max_i})$
end if

Algorithm 2. Novel outer feedback correction loop (OFCL).

power consumption profiles during the prediction stage as shown in Fig. 2. The following sections describe the details of the framework proposed.

3. State-space model for state-of-charge estimation in batteries

The proposed empirical state-space model is inspired by electric equivalent circuits for a battery cell. Previous research efforts have also used a state-space representation to describe the SOC evolution in time [4], although the parameterization that is proposed for the Open Circuit

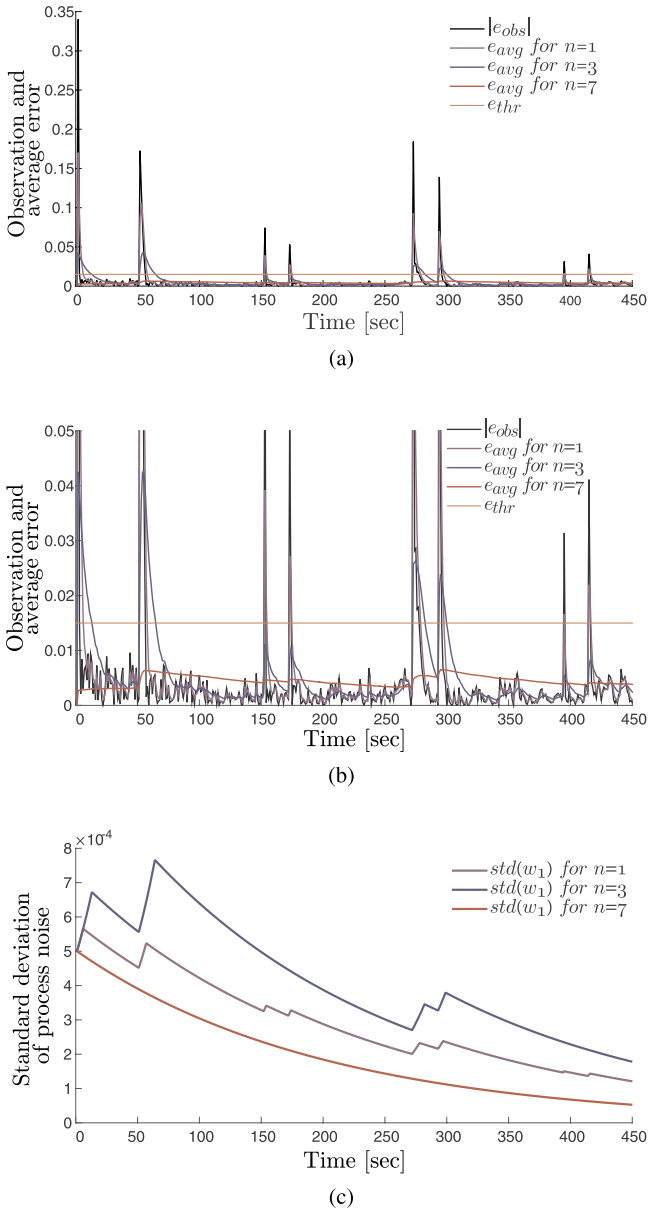

Fig. 5. Exemplification of the dynamics of the new OFCL for different values of *n*. (a) Absolute value of the current observation error and average observation error. (b) Wider view of the absolute value of the current observation error and average observation error. (c) Evolution of the standard deviation of the process noise over time.

Fig. 6. Multi-rotor platform used for validation. 3DR IRIS+ Quadcopter.

Table 2
Multi-rotor parameters.

Parameter	Symbol	Value	Units
Number of rotors	n	4	
Propeller diameter	D_p	0.2413	m
Total disc actuator area	A_t	0.1829	m^2
Empty mass	m_0	1.357	kg
Maximum payload mass	m_{pmax}	0.3	kg
Empty weight	W_0	13.2986	N
Maximum payload weight	W_{pmax}	2.94	N
Air density	ρ	1.15	kg/m^3

Table 3
Parameters of fitted curves.

i	a_i	b_i	c_i	d_i
0	0.07842	0.5	0.5493	0.5591
1	1.189	0.02347	− 0.01917	− 0.1106
2	− 0.06359	0.4004	1.127	− 0.03985
3	0.004595	0.0136	− 0.02208	− 2.577

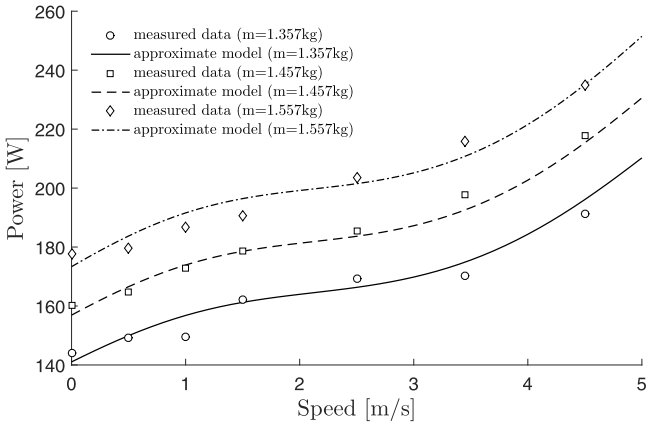

Fig. 7. Power required in climb.

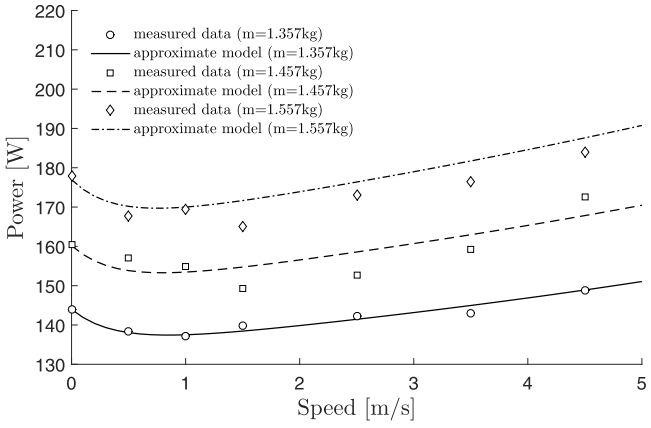

Fig. 8. Power required in descent.

Voltage (OCV) curve is insufficient for batteries of more than one cell.

On the other hand, battery performance is strongly determined by characteristics such as temperature or current discharge rate, which affect battery internal resistance and the total energy that the battery is able to deliver. In addition, battery internal resistance varies as a function of the State of Charge (SOC) [28]. Therefore, in order to incorporate the current load dependence, temperature dependence and SOC dependence; the proposed model uses the concept of artificial evolution [21,22] to estimate the absolute value of the battery internal

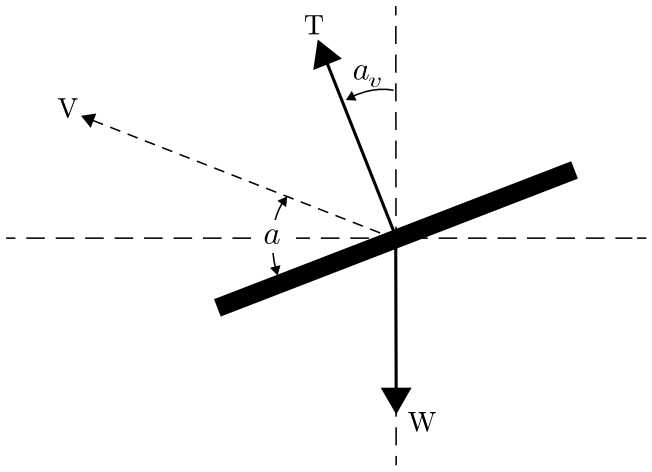

Fig. 9. Rotary-wing aircraft in forward flight.

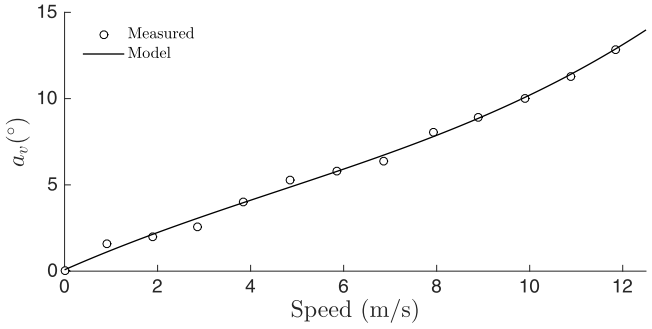

Fig. 10. Angle-of-attack in horizontal flight.

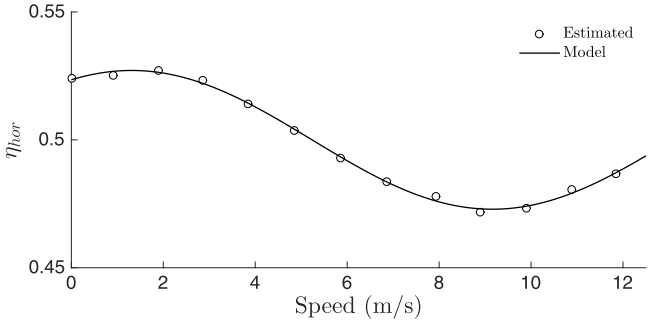

Fig. 11. Efficiency factor in horizontal flight.

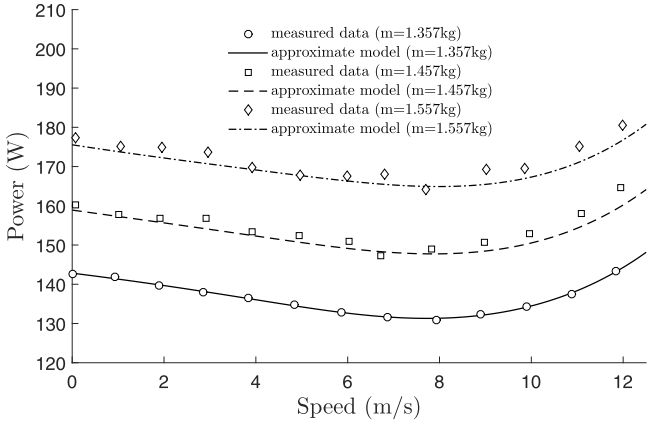

Fig. 12. Power required in horizontal flight.

resistance and the total energy delivered by the battery. Artificial evolution provides the mechanism for generating new parameter values at each time step by adding additional random disturbances to sampled state vectors. Its implementation is made by extending the dimension of the state vector and associating its first component with the value of this time-varying parameter.

The model (Eqs. (3)–(6)) assumes a discrete characterization of the dynamics of the battery, and the availability (in real time) of voltage and current measurements. The model structure provides a modification to the observation equation that incorporates most of the non-linearities found in OCV discharge curves, while simultaneously enabling the implementation of reliable off-line estimation procedures for the estimation of its parameters.

State transition model:

$$R_{int}(k+1) = R_{int}(k) + w_1(k) \tag{3}$$

$$SOC(k+1) = SOC(k) - P(k)\cdot\Delta t\cdot E_{crit}(k)^{-1} + w_2(k) \tag{4}$$

$$E_{crit}(k+1) = E_{crit}(k) + w_3(k) \tag{5}$$

Measurement equation:

$$V(k) = v_{oc}(k) - i(k)\cdot R_{int}(k) + \eta(k) \tag{6}$$

Where:

$$v_{oc}(k) = v_L + \lambda\cdot e^{\gamma\cdot SOC(k)} - \mu\cdot e^{-\beta\sqrt{SOC(k)}} \tag{7}$$

$$i(k) = \frac{v_{oc}(k) - \sqrt{v_{oc}(k)^2 - 4\cdot R_{int}(k)\cdot P(k)}}{2\cdot R_{int}(k)} \tag{8}$$

The power $P(k)$ (measured in Watts), and the sample time Δt (measured in seconds) are input variables (i.e., the input vector, $u(k)$), and the battery voltage $V(k)$ (measured in Volts) is the system output (i.e.,the output vector, $y(k)$). v_{oc} is the OCV (measured in Volts) and $i(k)$ is the discharge current (measured in Amps), which is calculated by solving the quadratic equation:

$$i(k) = \frac{P(k)}{v_{oc}(k) - i(k)\cdot R_{int}(k)} \tag{9}$$

$$0 = R_{int}(k)\cdot i(k)^2 - v_{oc}(k)\cdot i(k) + P(k) \tag{10}$$

The parameters are defined as $R_{int}(k)$, the internal resistance, and $E_{crit}(k)$, the expected total energy delivered by the battery (i.e., the unknown parameter vector, $\theta(k)$). The only state, $SOC(k)$, the State of Charge, is defined as the remaining battery energy normalized by E_{crit} (i.e., the state vector, $x(k)$). Process (w_1, w_2 and w_3) and measurement (η) noises (i.e., the process noise vector $v(k)$ and measurement noise vector $n(k)$) are assumed Gaussian. It is important to mention that process noise w_2 is correlated with η, the measurement noise because the evolution in time of state $SOC(k)$ depends on voltage measurements. The quantities v_L, λ, γ, β, and μ are model parameters to be estimated off-line. The initial SOC, $SOC(k_0)$, is suggested to be estimated before starting the discharge by measuring the OCV and computing the inverse of the Eq. (7). The initial internal resistance, $R_{int}(k_0)$, and the initial total energy, $E_{crit}(k_0)$, can also be estimated off-line assuming they are constants. It should be mentioned that these latter parameters are considered constant only during the off-line procedure to estimate the parameters, but during the estimation process, artificial evolution generates new values for these parameters at each time step.

The procedure to estimate the parameters is basically a curve fitting between the measured voltage during a discharge at variable current and the voltage obtained with the model, as shown in Fig. 3. Since the internal resistance is assumed to be constant without considering SOC dependence, the curve fitting at the beginning of the discharge cycle (when the internal resistance should be larger) is less accurate. Nevertheless, the value estimated off-line provides an average value of the internal resistance for different values of load current. The

Table 4
Flight Plan No. 1.

No.	Maneuver	Payload (kg)	Translational speed (m/s)	Duration (s)
1	Take off & Climb (to 120 m)	0.3	1.5	80
2	Horizontal flight	0.3	6.0	210
3	Descent & land	0.3	0.5	240
4	Delivering payload	0.3	0.0	60
5	Take off & Climb (to 120 m)	0.0	1.5	80
6	Horizontal flight	0.0	6.0	210
7	Descent & land	0.0	0.5	240
8	Fully deplete battery	–	–	Until reaching the voltage threshold

Table 5
OFCL parameters

Parameter	Value
n	3
e_{thr}	0.0329
p	[0.995 0.99 0.995]
q	[1.025 1.01 1.025]

parameters found are shown in Table 1 which correspond to a 3S 5100mAh Li–Po battery. The model is validated for 1C, 3C and 4C rate discharges as shown in Fig. 4.

4. Outer feedback correction loop

Artificial evolution provides the mechanism for generating new parameter values at each time step by adding random disturbances (process noise) to sampled state vectors, and thus it allows incorporating effects on the battery performance that are not directly included in the model. However, the process noise must be large enough to ensure convergence, but small enough to ensure precise tracking. Nevertheless, as process noise increases, the uncertainty on the state/parameter estimate increases as well, which affects the prediction results. Therefore, an Outer Feedback Correction Loop (OFCL) is proposed to increase the process noise when detecting inconsistencies between measurements and estimations of the output (i.e., observation error) so that it is possible to ensure convergence, and to decrease the process noise when convergence has been reached and there are no significant inconsistencies between measurements and estimations of the output.

The voltage in the battery does not have considerable variations in small intervals of time (less than 30 s) during almost all the discharge cycle. Even more, the typical voltage drop that the battery undergoes during small time intervals, due to changes in the SOC, is comparable to the observation noise. In this regard, short-term predictions are not enough to evaluate the performance of the model. Therefore, the OFCL by Tampier et al. [29] (Algorithm 1) uses the accumulated observation error to take into account the error in the previous time horizons.

However, this OFCL results in unnecessary increases of the standard deviation of the process noise. The accumulated observation error frequently reaches the threshold, causing an increase in the standard deviation of the process noise, even when the observation error remains at acceptable values. In addition, the standard deviation of the process noise is increased only at the instant when accumulated error reaches the threshold. When this happens, the accumulated error is set to zero again, which means that in the next time step the accumulated error could be less than the threshold and the standard deviation could quickly decline again. Consequently, the effective increase of the deviation may not be sufficient.

Therefore, the proposed OFCL here is based on long-term results, but instead of using the accumulated error, it uses a metric inspired by congestion control and Active Queue Management (AQM) techniques for IP networks, i.e., communication networks that use Internet Protocol (IP). Similar to the problem we are dealing with here, it is not convenient in IP networks to make decisions about packet drop (i.e., discard incoming packets to the queue in the server) based on short-term behaviour of the queue size in the server, because the queue size is fluctuating and is subject to several sources of uncertainties, such as the occurrence of packet arrivals to the queue, the number of traffic sources, the type of traffic (continuous or burst), among other. In particular, this new OFCL uses the metric defined in [30] for *Cisco Systems* equipment as shown in Algorithm 2, where n is the exponential weight factor, a user-configurable value. For high values of n, the previous average becomes more important. If the value of n gets too high, the OFCL will not react to large observation errors. The standard deviation of the process noise will be affected only in decreasing order. For low values of n, the average error closely tracks the current observation error. If the value of n gets too low, the OFCL will overreact to large instantaneous observation errors and unnecessarily will increase the standard deviation of the process noise. In other words, this algorithm implements a basic digital filter on the observation error. See Fig. 5.

e_{obs} is the observation error (the difference between the acquired measurement for the output and the one expected by the estimation algorithm), e_{avg} is a weighted average of the previous observation errors, with initial value of zero, e_{thr} is the decision threshold to modify the process noise. If average error is lower than the threshold, the standard deviation of the process noise is reduced, but if it is larger than the threshold, it increases. Also p_i are constants with values between 0 and 1 for the i^{th} state/parameter, while q_i are constants bigger than 1. Finally, std_{min_i} are the lower bounds which indicate the minimum standard deviation value accepted, and std_{max_i} are the upper bounds which indicate the maximum standard deviation value accepted. Finally, with the proposed OFCL, the decision threshold intuitively can be defined as a value equal to or less than the standard deviation of the observation noise.

5. Approximate power consumption model for rotary-wing aircraft

The ideal power consumption is characterised through a rough model based on aerodynamic equations for each flight maneuver (climb, hover, horizontal flight and descent). The aerodynamic-based model determined in this work is based on momentum theory [31], which uses the simplest model of thrust generation. Therefore, it is an approximate model that provides a practical way to calculate the ideal power consumption for a flight plan previously known, as a function of the weight, disc actuator area, air density, translational speed and the type of manoeuvre. The temperature effects are indirectly included in the air density, the humidity effects are not considered, and also it is assumed that the wind speed is moderate.

According to Stepniewski [31], the ideal power required by a rotary-wing aircraft with single rotor (helicopter) in hovering, is given by:

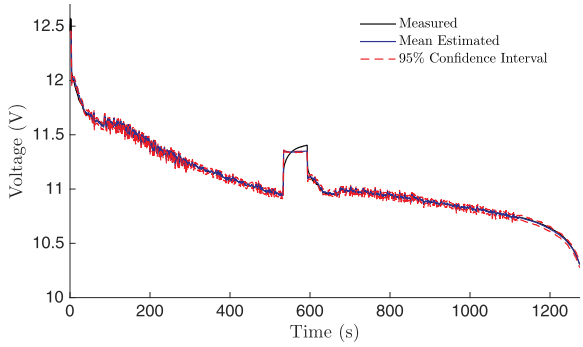

(a) Estimated Voltage

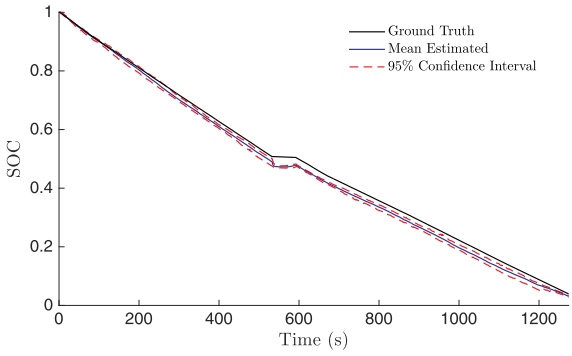

(b) Estimated SOC

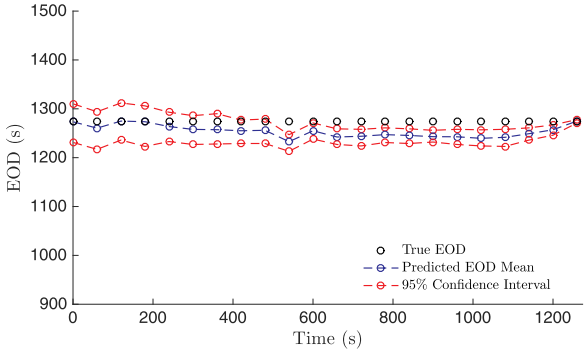

(c) Predicted EOD

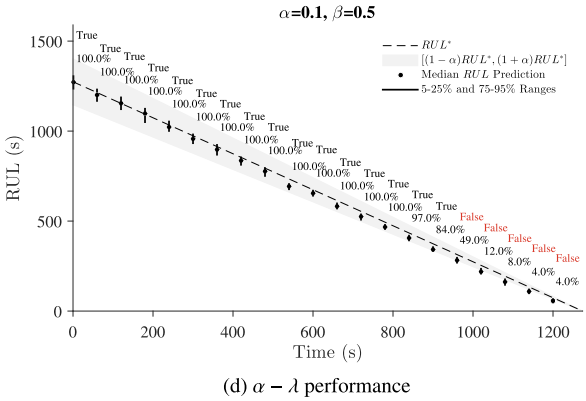

(d) $\alpha - \lambda$ performance

Fig. 13. Equivalent Circuit Model, SOC estimation with PF and EOD prediction with MC.

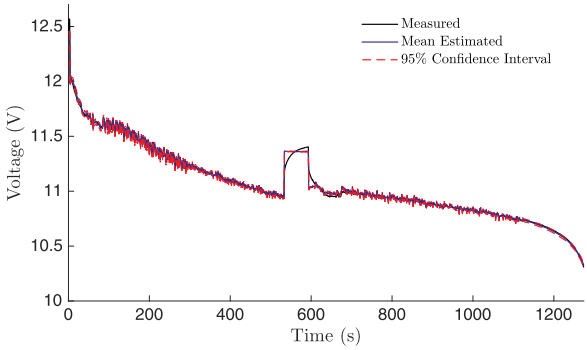

(a) Estimated Voltage

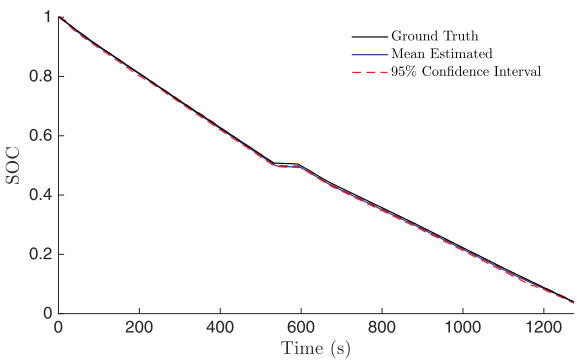

(b) Estimated SOC

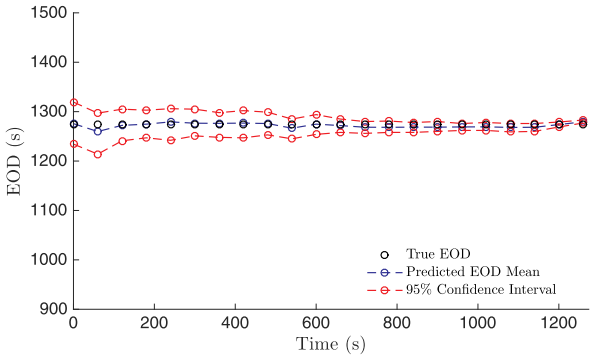

(c) Predicted EOD

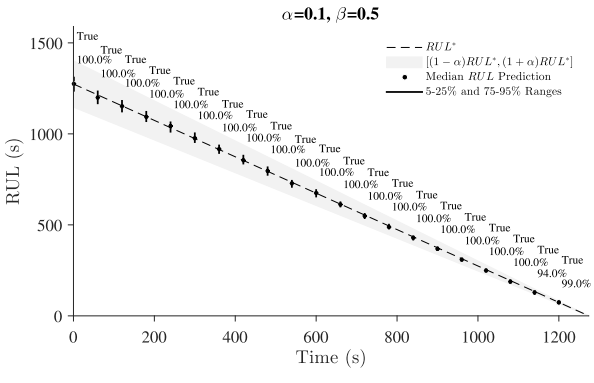

(d) $\alpha - \lambda$ performance

Fig. 14. Equivalent Circuit Model, SOC estimation with PF + OFCL and EOD prediction with MC.

Table 6
Average prediction results of 50 realizations

SOC	Equivalent Circuit Model, PF estimator and MC predictor			Equivalent Circuit Model, PF + OFCL estimator and MC predictor			Electrochemistry-based Model, PF estimator and MC predictor		
	$\hat{EOD}$	$JITP_{5\%}$	$\pi[r(k)]\|_{\alpha^-}^{\alpha^+}$	$\hat{EOD}$	$JITP_{5\%}$	$\pi[r(k)]\|_{\alpha^-}^{\alpha^+}$	$\hat{EOD}$	$JITP_{5\%}$	$\pi[r(k)]\|_{\alpha^-}^{\alpha^+}$
75% (t = 267 s)	1271.301 s	1242.380 s	100.00%	1276.178 s	1248.960 s	100.00%	1302.814 s	1238.160 s	99.78%
50% (t = 598 s)	1262.072 s	1247.560 s	100.00%	1270.857 s	1255.960 s	100.00%	1306.470 s	1254.740 s	94.80%
25% (t = 959 s)	1245.874 s	1229.580 s	60.00%	1263.704 s	1256.800 s	100.00%	1316.338 s	1281.600 s	22.84%

$$P_{id_h} = \frac{W^{3/2}}{\sqrt{2A\rho}}, \tag{11}$$

where ρ is air density, W is the total weight of the aircraft equal to the empty-operative weight W_0 plus the payload weight W_p, A is the total disc actuator area; namely, πR^2, where R is the rotor or slipstream radius. The parameter values for the multi-rotor platform used for validation, namely, a 3DR IRIS+ quadcopter (Fig. 6) are summarized in the Table 2.

To extend the Eq. (11) to n-rotors, Gatti et al. [3] assumes that the total weight is equally distributed on n-rotors, and that A_t is the sum of the n-disc actuator areas. Taking the preceding assumptions, and based on the equations in [31], this work here proposes the following equations for the power required by rotary-wing aircraft with n-rotors, in hovering P_h, climb P_c, and descent P_d:

$$P_h = \frac{W^{3/2}}{\eta_h \cdot \sqrt{2\rho A_t}}, \tag{12}$$

$$P_c = \frac{W}{\eta_c(V_c)}\left(\frac{V_c}{2} + \sqrt{\frac{V_c^2}{4} + \frac{W}{2\rho A_t}}\right), \tag{13}$$

$$P_d = \frac{W}{\eta_d(V_d)}\left(\frac{-V_d}{2} + \sqrt{\frac{V_d^2}{4} + \frac{W}{2\rho A_t}}\right), \tag{14}$$

where V_c is the vertical climb speed, V_d is the vertical descent speed, and η is the efficiency factor of the propulsion system (electric speed controller (ESC), motors, propellers), which slowly varies as a function of the rotor thrust, among other factors. This work defines η_c, the efficiency factor in climb, and η_d, the efficiency factor in descent, as functions of the climb speed and descent speed respectively. The following curves for the efficiency factors are proposed:

$$\eta_c(V_c) = c_0 + c_1 \cdot \cos(V_c \cdot c_2) + c_3 \cdot \sin(V_c \cdot c_2) \tag{15}$$

$$\eta_d(V_d) = d_0 \cdot \exp(V_d \cdot d_1) + d_2 \cdot \exp(V_d \cdot d_3) \tag{16}$$

The parameters of the above curves (see Table 3) are computed by a curve fitting with the power consumed in climb and descent by the quadcopter without payload ($m_p = 0$ g) at different speeds. Then, Eqs. (12)–(14) are validated for $m_p = 100$ g and $m_p = 200$ g as shown in Figs. 7 and 8. Note that the mass of the quadcopter without payload, m_0, is 1.357 kg, so that the total mass with a payload of 100 g is 1.457 kg, and 1.557 kg with a payload of 200 g.

For the horizontal flight case, another assumption is made for simplification: The rotor tilt, a_v, required in steady flight at low velocities is assumed to be negligible such that $a_v \approx 0$ and $T \approx W$ (See Fig. 9). The average maximum speed of a small-size multirotor is about 15 m/s, and several applications just need speeds up 5 m/s. For example, in land surveys, the usual speed in forward flight is set to 3 m/s so that the aerial photo taken are not blurry. With this in mind, the assumptions above are sufficient.

Since $T \approx W$, the power required in horizontal flight, P_{hor}, where $a_v = a \approx 0$, for a rotary-wing aircraft moving in the gravitational coordinate system at velocity of flight V_{hor}, is roughly given by:

$$P_{hor} = \frac{W}{\eta_{hor}(V_{hor})}(V_{hor}\sin(a_v(V_{hor})) + v_{hor}), \tag{17}$$

where v_{hor}, the induced velocity in horizontal flight, is given by:

$$v_{hor} = \sqrt{-\frac{V_{hor}^2}{2} + \sqrt{\frac{V_{hor}^4}{4} + \left(\frac{W}{2\rho A_t}\right)^2}} \tag{18}$$

The angle-of-attack, a_v, and the efficiency factor in horizontal flight, η_{hor}, are proposed to be modelled as a function of the translational speed as described by Eqs. (19) and (20), respectively. The parameters of the curves proposed (see Table 3) for horizontal flight are estimated by a curve fitting (Figs. 10 and 11) using the measured angle-of-attack and the measured values of the power consumed by the quadcopter without payload at different speeds. Then, Eq. (17) is validated for $m_p = 100$ g and $m_p = 200$ g as shown in Fig. 12.

$$a_v(V_{hor}) = a_0 + a_1 \cdot V_{hor} + a_2 \cdot V_{hor}^2 + a_3 \cdot V_{hor}^3 \tag{19}$$

$$\eta_{hor}(V_{hor}) = b_0 + b_1 \cdot \cos(V_{hor} \cdot b_2) + b_3 \cdot \sin(V_{hor} \cdot b_2) \tag{20}$$

6. Results & discussion

The discharge cycle data used in this study corresponds to a delivery mission performed by a 3DR IRIS+ quadcopter whose flight plan is composed of the phases in Table 4. Phase 8 consists in discharge of the battery at a similar power to that observed during phase 6 to safely obtain an approximate measurement for the amount of flight time that would have been supported by the battery if the multicopter had continued to be flown at the approximately same speed as it was going in phase 6. This measurement allows comparison between battery EOD predictions made at various points over the sample mission, and the EOD time observed experimentally, which is 1274 s for a voltage threshold (V_{EOD}) equal to 10.3 volts.

Performance indicators for prognostics used in this analysis incorporate information from EOD expectations, which correspond to the instant k when the expectation of the battery voltage reaches the threshold, the Just-In-Time Point value which incorporates the concept of risk, specifying the cycle of operation where the probability of failure reaches a specified threshold γ ($JITP_{\gamma\%}$) [32], and the $\alpha - \lambda$ performance with the β criterion [33,34]:

$$\hat{EOD} \triangleq E\{k | E\{V(k)\} = V_{EOD}\}, \tag{21}$$

$$JITP_{\gamma\%} = \underset{eod}{\operatorname{argmin}}(Pr\{EOD \le eod\} \ge \gamma\%), \tag{22}$$

$$\pi[r(k)]\|_{\alpha^-}^{\alpha^+} = \sum_{\alpha^-}^{\alpha^+} \phi(x), \tag{23}$$

where $r(k)$ is the probability distribution of the predicted RUL at time index k, ϕ is the non-parameterized probability distribution, and π is the total probability mass within $[\alpha^-, \alpha^+]$, being $\alpha^- = RUL^*(1-\alpha)$, $\alpha^+ = RUL^*(1+\alpha)$ and RUL^* the ground truth RUL. RUL distribution satisfies β criterion when $\pi[r(k)]\|_{\alpha^-}^{\alpha^+} \ge \beta$.

A Particle Filter (PF) with 100 particles is used as estimation

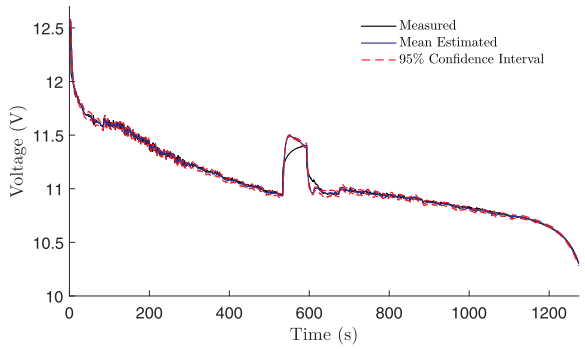

(a) Estimated Voltage

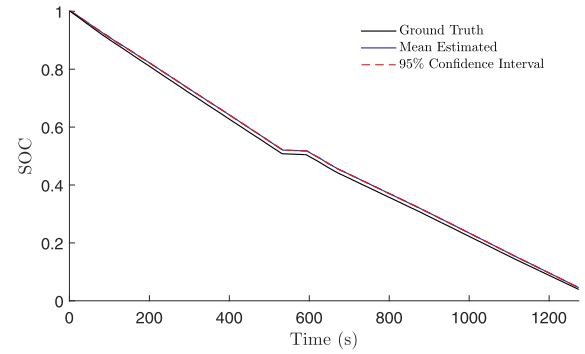

(b) Estimated SOC

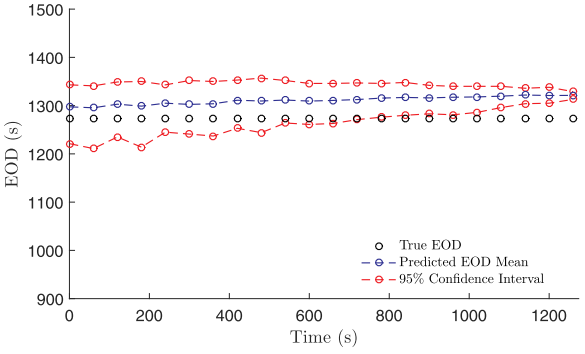

(c) Predicted EOD

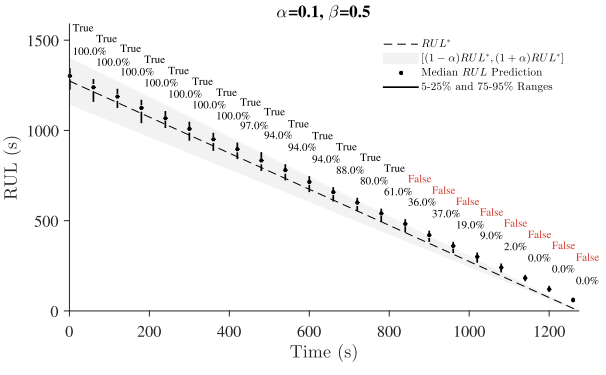

(d) $\alpha - \lambda$ performance

Fig. 15. Electrochemistry-based model, SOC estimation with PF and EOD prediction with MC.

Table 7
Average estimation processing time per iteration.

Algorithm	Equivalent Circuit Model	Electrochemistry-based Model
UKF	$1.309e-3$ s	$1.993e-3$ s
PF ($N = 100$)	$6.508e-4$ s	$2.450e-3$ s

Table 8
MC average processing time for a time windows of 1274 s.

Samples	Equivalent Circuit Model	Electrochemistry-based Model
10	0.464 s	0.811 s
50	0.483 s	1.570 s
100	0.496 s	2.510 s
500	0.637 s	10.155 s
1000	0.821 s	18.656 s
5000	1.994 s	42.208 s
10,000	3.279 s	67.313 s
50,000	16.584 s	306.517 s
100,000	32.558 s	609.249 s

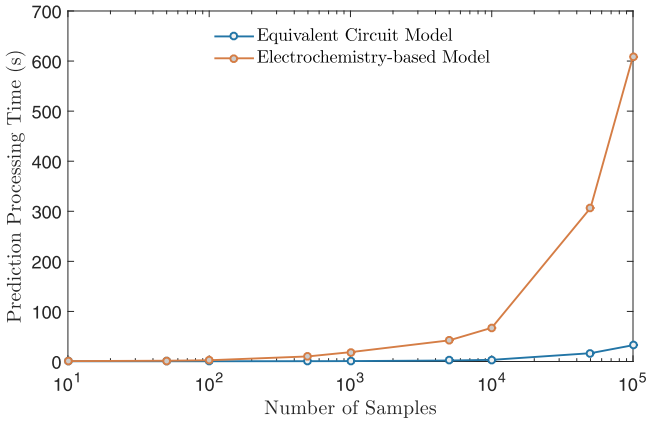

Fig. 16. MC processing time for a time windows of 1274 second.

algorithm and Monte Carlo (MC) with 100 samples is used as prediction algorithm. The number of particles and samples have been chosen to keep an efficient but accurate approach. There is evidence in [35] which indicates that for energy storage devices, there is no further benefit from the point of view of the effectiveness of the algorithm if the number of particles and samples are increased to 200 or more. In order to insulate the sources of uncertainty from the uncertainty associated to the future inputs, the actual power profile was used as future input during the prediction stage.

Having established the above, this analysis is divided into three parts. Firstly, to evaluate the effectiveness of the OFCL, SOC estimation and EOD prediction without and with the OFCL proposed were performed. The OFCL parameters used are summarized in Table 5. The results of SOC estimation and EOD prediction without and with OFCL are shown in Figs. 13 and 14 correspondingly, and the average results of 50 realizations in terms of the above metrics are summarized in Table 6.

EOD estimates presented in Table 6, show that the EOD expectation is, indeed, a random variable. Furthermore, it may happen that some realisations of this random variable underestimate (or overestimate) the ground truth EOD. Nevertheless, the obtained estimates when the equivalent circuit model is used, are sufficiently accurate. More importantly, they tend to underestimate the EOD, thus minimising the probability of unexpected failure (conservative approach).

The maximum error in the expected EOD time value is 28 s for the first case without OFCL, and 19 for the second case with OFCL, when the prediction horizon was 315 s. Considering the length of the long-

Table 9
Flight Plan No. 2.

No.	Maneuver	Payload (kg)	Translational-speed (m/s)	Duration (s)
1	Take off & Climb (to 120 m)	0.3	2.5	48
2	Horizontal flight	0.3	12.0	360
3	Descent & land	0.3	1.5	80
4	Delivering payload	–	0.0	60
5	Take off & Climb (to 120 m)	0.0	2.5	48
6	Horizontal flight	0.0	12.0	360
7	Descent & land	0.0	1.5	80
8	Fully deplete battery	–	–	Until reaching the voltage threshold

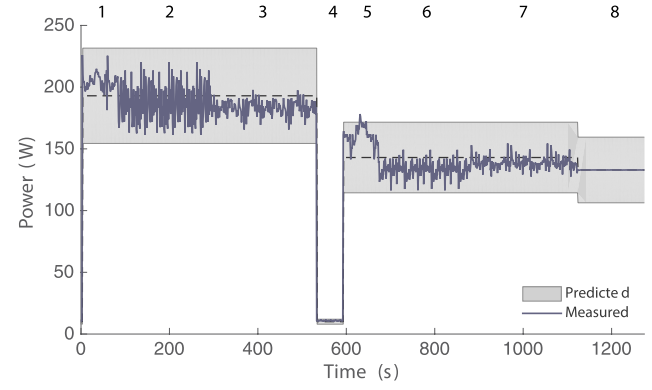

(a) Power profile for flight plan No. 1. Measured and predicted.

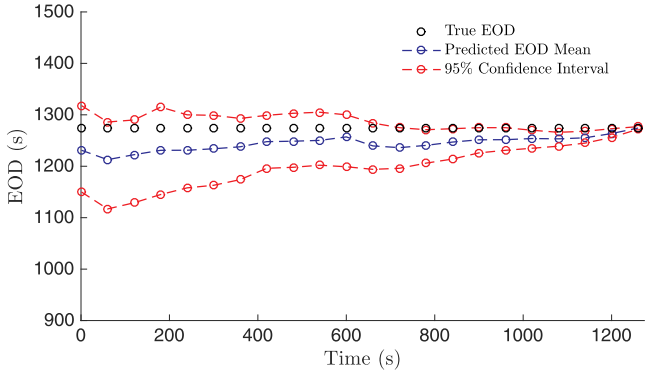

(b) Predicted EOD

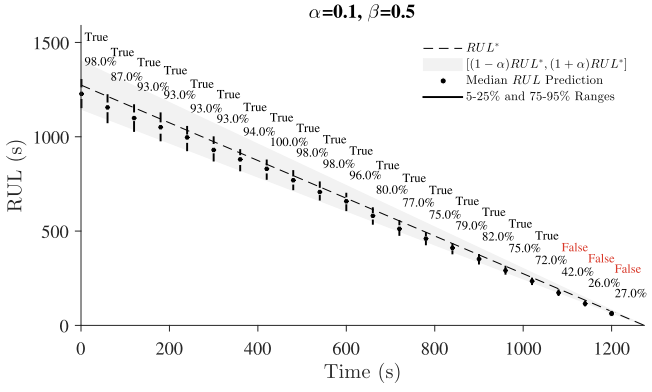

(c) $\alpha - \lambda$ performance

Fig. 17. Equivalent circuit battery model, estimation with PF + OFCL and prediction with MC and future inputs for flight plan No. 1 defined by the hover equation plus ± 20%.

term prediction windows, the maximum error between the ground truth and the expected EOD correspond to only 8.88% and 6.3% respectively. Regarding Just-In-Time Point estimates, the values obtained for the $JITP_{5\%}$ when the equivalent circuit model is used are always smaller than the ground truth EOD, thus ensuring a safe utilisation of the asset. In terms of the $\alpha - \lambda$ performance, the average of the probability mass, π, is 86.6% for the first case, while in the second case it is 100%.

In general, reasonable results were obtained in the first scenario without OFCL, and improved results in the second case with the proposed OFCL that implements a digital filter on observation error instead of using the accumulated error. This supports the idea that an OFCL helps to diminish the bias in Bayesian state estimation, which results in more accurate prediction results since the states/parameters estimated correspond to the initial states/parameters of the prediction stage.

Secondly, it is of interest to evaluate the proposed solution in terms of effectiveness and efficiency. To achieve it, SOC estimation and EOD predictions are also performed using a high fidelity battery model. The prediction results are compared using the above metrics to evaluate the effectiveness while the processing time during estimation and prediction processes are measured in order to evaluate the efficiency. The model used is a Electrochemistry-based model [24] of lithium-ion batteries that capture the significant electrochemical processes.

For implementation, models and algorithms of the Prognostics Model Library [36] and the Prognostics Algorithm Library [27] by NASA Ames Research Center were used for the development of this study. MATLAB R2015b running on a Intel Core i7-2860QM CPU @ 2.50Ghz with 8GB of RAM was used to measure the processing times, making sure no other application was running at the same time.

The results of SOC estimation and EOD prediction using the Electrochemistry-based model are shown in Fig. 15, and the average results of 50 realizations are summarized in Table 6. The average estimation processing time per iteration was measured for both models using Unscented Kalman Filter (UKF) and Particle Filter (PF) as estimation algorithms. See Table 7. Similarly, the prediction processing time for a time window prediction of 1274 s using both models and MC as prediction algorithm was measured for different number of samples. The results are summarized in Table 8 and Fig. 16.

Results with the electrochemistry-based model tend to slightly overestimate the EOD as reported by Daigle and Kulkarni [24] for variable loading discharges. In this case, the maximum error in expected EOD time value is 42 s, that occurs when the prediction horizon is 315 s. Considering the length of the long-term prediction window, the maximum error between the ground truth and the expected EOD correspond to 13.3%. Regarding Just-In-Time Point estimates, the values obtained for the $JITP_{5\%}$ are not always smaller than the ground truth EOD, which does not provide a safe utilisation of the asset because the actual EOD time may be before end of mission. In terms of the $\alpha - \lambda$ performance, the average of the probability mass, π, is 72.47%.

The use of the electrochemistry-based model results in reasonable but less accurate results compared to the results obtained using the equivalent circuit model, despite electrochemistry-based model providing a more detailed characterization of the underlying battery

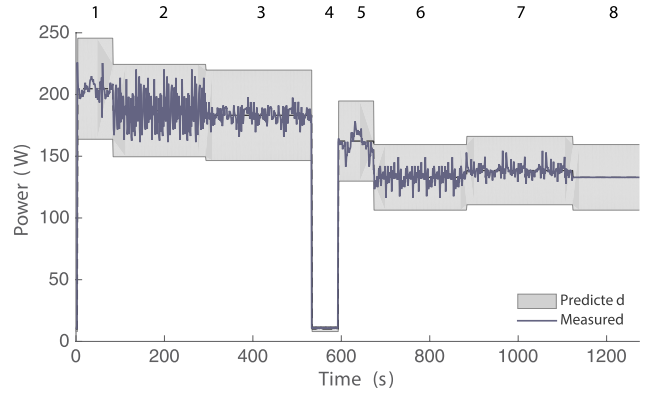

(a) Power profile for flight plan No. 1. Measured and predicted.

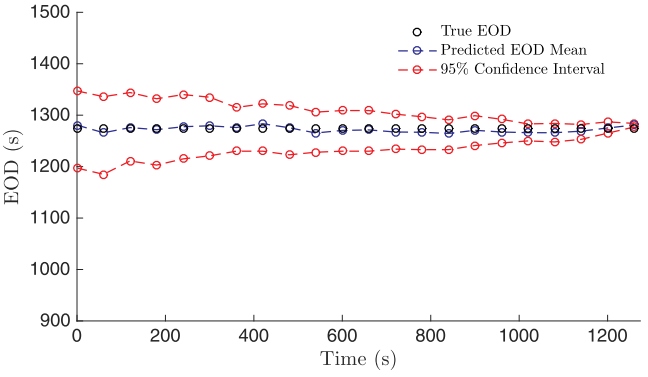

(b) Predicted EOD

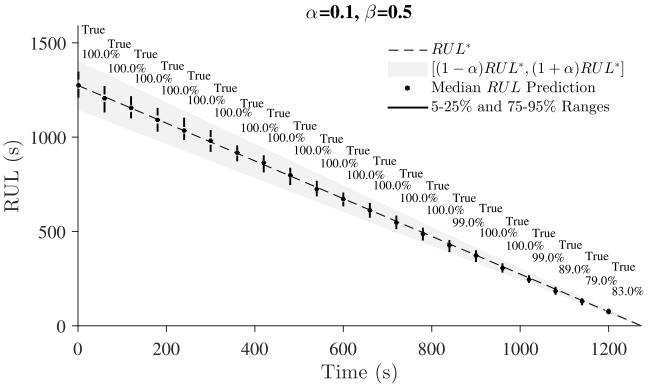

(c) $\alpha - \lambda$ performance

Fig. 18. Equivalent circuit battery model, estimation with PF + OFCL and prediction with MC and future inputs for flight plan No. 1 defined by the power consumption model plus ± 20%.

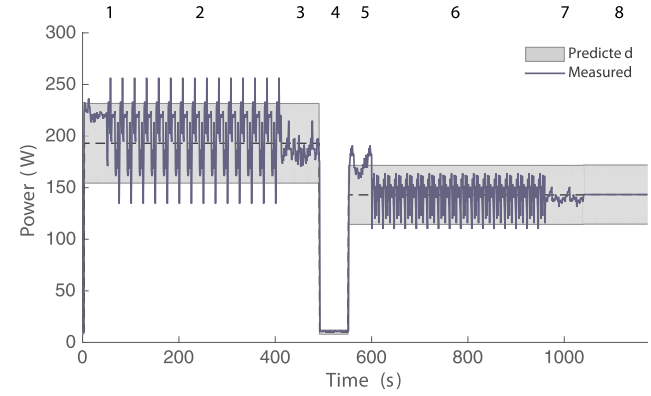

(a) Power profile for flight plan No. 2. Measured and predicted

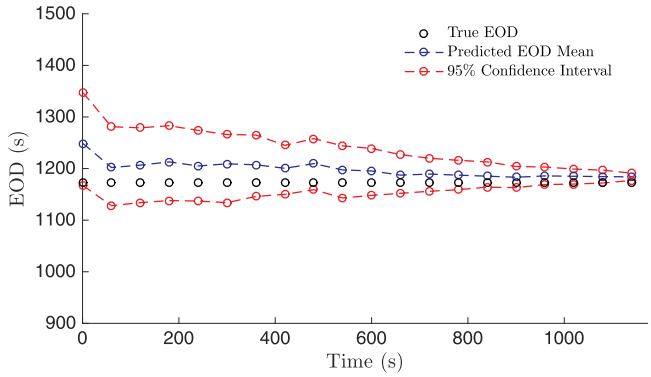

(b) Predicted EOD

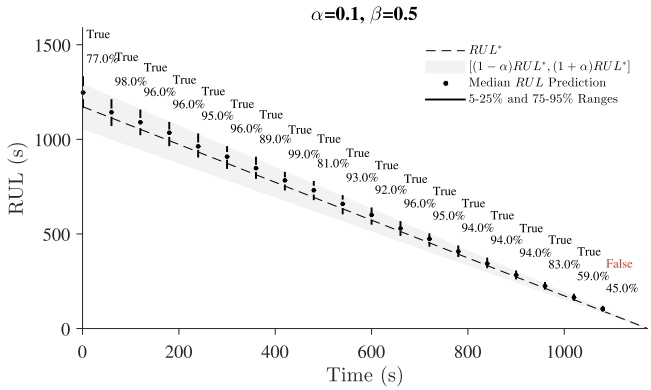

(c) $\alpha - \lambda$ performance

Fig. 19. Equivalent circuit battery model, estimation with PF + OFCL and prediction with MC and future inputs for flight plan No. 2 defined by the hover equation plus ± 20%.

phenomena. This is attributed to the difficulty associated with proper estimation of model parameters that meet the constraints of the model. In particular, the electrochemical-based model requires 27 parameters that must be estimated through several stages using different discharges. In contrast, the equivalent circuit model requires only 7 parameters which are estimated through a single stage using a single discharge.

The estimation processing time per iteration (see Table 7) using the equivalent circuit model is 65% of the time per iteration using the electrochemistry-based model when UKF is used as estimation algorithm, and it is 26.5% of the time per iteration using the electrochemistry-based model when PF with 100 particles is used as estimation algorithm. Considering that PF is shown to be more accurate than UKF [17], the possibility of using PF without increasing the processing times constitutes an advantage when one deals with constrained processing power, which may be encountered on small UAVs.

The prediction processing times are also shown significantly lower when the equivalent circuit model is used, in particular when the number of samples increases. As can be seen in Table 8 and Fig. 16, the prediction processing times with 10^2 and 10^5 samples using the equivalent circuit model is 19.76% and 5.34%, respectively, of the prediction processing time using the electrochemistry-based model. This could be attributed to the number of states of the model. The equivalent circuit model has 3 states in contrast to the electrochemistry-based model that has 7 states. Also, the electrochemistry-based model contains complex mathematical operations, such as logarithmic and

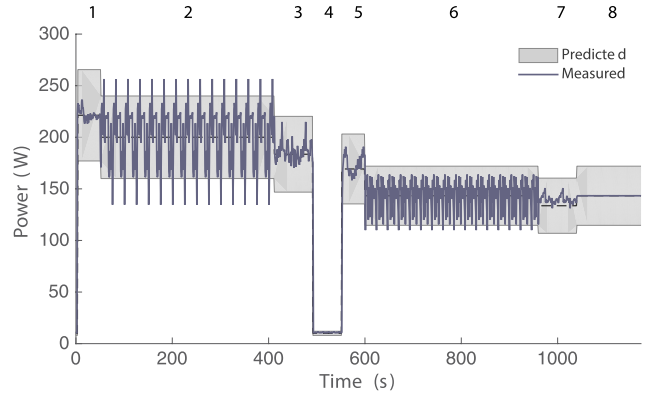

(a) Power profile for flight plan No. 2. Measured and predicted

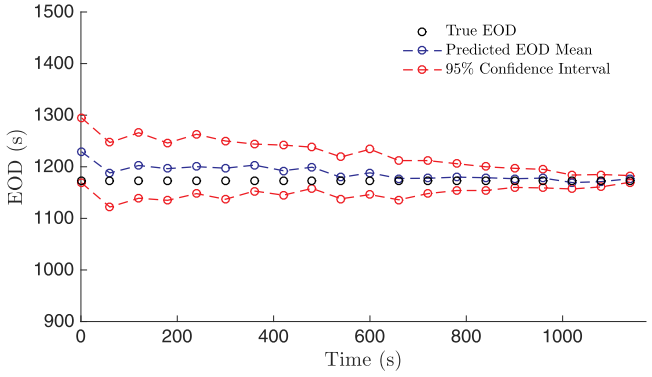

(b) Predicted EOD

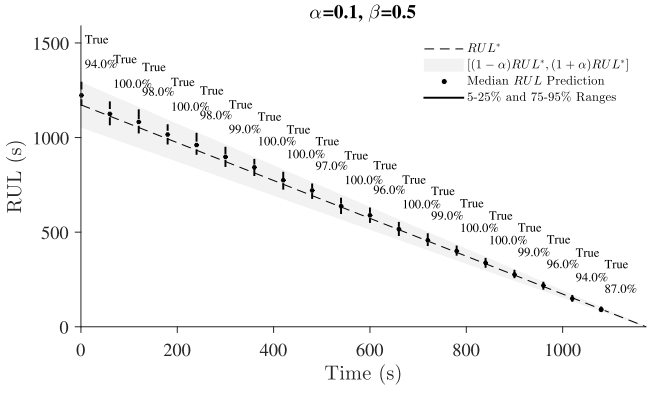

(c) $\alpha - \lambda$ performance

Fig. 20. Equivalent circuit battery model, estimation with PF + OFCL and prediction with MC and future inputs for flight plan No. 2 defined by the power consumption model plus ± 20%.

inverse hyperbolic functions, that require higher computational resources.

Finally, instead of using the actual future inputs, the proposed power consumption model is used to evaluate its effects on prediction results.

An analytical framework for addressing the flight time estimation of rotary-wing aircraft is proposed in [3] through an analysis of the balance between available and required power. This latter is described by Eq. (12) and assumes that the aircraft is in hovering flight condition during the entire flight, which is inaccurate and might cause a bias in the estimation of the flight time. By using the power consumption model proposed in the work described herein (Eqs. (12), (13), (14) and (17)) it is expected to get more accurate EOD prediction given a flight plan.

To validate this, SOC estimation and EOD predictions have been performed for two flight plans described in Tables 4 and 9, firstly only using P_h ± 20% as future inputs, and secondly, using $P_{h,\ c,\ d,\ hor}$ ± 20% as future inputs as shown in Figs. 17 and 18 for the first flight plan, and in Figs. 19 and 20 for the second flight plan.

As shown in Figs. 17–20, when the aerodynamic-based model is used to define the future inputs, the prediction results are more accurate and stable. In addition, the bias in the expected EOD is lower and the confidence intervals are narrower, which causes the $\alpha - \lambda$ performance values to improve relative to the prediction results obtained when only the hover equation is implemented. Depending on the flight plan, using only the hover equation to define the future inputs might cause underestimates of the EOD as seen for flight plan No. 1, or overestimates of the EOD as seen for flight plan No. 2.

7. Conclusions

This work addresses a gap in BHM systems for rotatory-wing UAVs that have constraints associated with weight, size, and cost. To reduce computational resources without losing accuracy, this study presents a model-based prognostic framework for batteries in small-size multirotors that uses a simplified battery model, a novel OFCL during the estimation stage, and an aerodynamic-based characterization of the future power consumption profiles used during the prediction stage. Results show that the proposed framework is able to track the voltage well and provides very accurate EOD predictions while being computationally efficient. While the current framework uses a uniform distribution to characterize the uncertainty on the future power consumption, future work should include a more detailed characterization of the uncertainty on the future inputs associated with wind speed and wind direction since wind conditions affect aircraft performance and power consumption.

References

[1] Handbook of Unmanned Aerial Vehicles. Valavanis KP, Vachtsevanos GJ, editors. 1Springer Netherlands; 2015.
[2] Meyer J, du Plessis F, Clarke W. Aerial Vehicles. University Johannesburg, South Africa: InTech, Chapters published; 2009. p. 443–97. Chapter: Design Considerations for Long Endurance Unmanned Aerial Vehicles
[3] Gatti M, Giulietti F, Turci M. Maximum endurance for battery-powered rotary-wing aircraft. Aerosp. Sci. Technol. 2015;45:174–9. https://doi.org/10.1016/j.ast.2015.05.009. http://www.sciencedirect.com/science/article/pii/S127096381500156X
[4] Pola D, Navarrete H, Orchard M, Rabie R, Cerda M, Olivares B, et al. Particle-filtering-based discharge time prognosis for lithium-ion batteries with a statistical characterization of use profiles. Reliab., IEEE Trans. 2015;64(2):710–20. https://doi.org/10.1109/TR.2014.2385069.
[5] Saha B, Quach P, Goebel K. Exploring the model design space for battery health management. Proceedings of the Annual Conference of the Prognostics and Health Management Society. Montreal, Canada. 2011.
[6] Saha B, Quach C, Goebel K. Optimizing battery life for electric UAVs using a Bayesian framework. Aerospace Conference, 2012 IEEE. 2012. p. 1–7. https://doi.org/10.1109/AERO.2012.6187365.
[7] Cuong Q, Bole B, Hogge E, Vazquez S, Daigle M, Celaya J, et al. Battery charge depletion prediction on an electric aircraft. Annual Conference of the Prognostics and Health Management Society 2013. 2013.
[8] Bole B, Daigle M, Gorospe G. Online prediction of battery discharge and estimation of parasitic loads for an electric aircraft. Annual Conference of the Prognostics and Health Management Society 2014. 2014.
[9] de Souza Candido A, Kawakami Harrop Galvao R, Yoneyama T. Control and energy management for quadrotor. Control (CONTROL), 2014 UKACC International Conference on. 2014. p. 343–8. https://doi.org/10.1109/CONTROL.2014.6915164.
[10] Hogge EF, Bole BM, Vazquez SL, Celaya JR, Strom TH, Hill BL, et al. Verification of a remaining flying time prediction system for small electric aircraft. Annual Conference of the Prognostics and Health Management Society 2015. 2015.
[11] Plett GL. Extended Kalman filtering for battery management systems of lipb-based hev battery packs: part 3. State and parameter estimation. J. Power Sources 2004;134(2):277–92. https://doi.org/10.1016/j.jpowsour.2004.02.033.
[12] Hu C, Youn BD, Chung J. A multiscale framework with extended Kalman filter for lithium-ion battery {SOC} and capacity estimation. Appl. Energy 2012;92:694–704. https://doi.org/10.1016/j.apenergy.2011.08.002. http://www.sciencedirect.com/science/article/pii/S0306261911004971
[13] Barbarisi O, Vasca F, Glielmo L. State of charge Kalman filter estimator for automotive batteries. Control Eng. Pract. 2006;14(3):267–75. https://doi.org/10.1016/j.conengprac.2005.03.027. Advances in Automotive Control (AC'04)Advances in

Automotive Control (AC'04), http://www.sciencedirect.com/science/article/pii/S0967066105001073
[14] Xing Y, He W, Pecht M, Tsui KL. State of charge estimation of lithium-ion batteries using the open-circuit voltage at various ambient temperatures. Appl. Energy 2014;113:106–15. https://doi.org/10.1016/j.apenergy.2013.07.008. http://www.sciencedirect.com/science/article/pii/S0306261913005746
[15] Zhang J, Xia C. State-of-charge estimation of valve regulated lead acid battery based on multi-state unscented kalman filter. Int. J. Electr. Power Energy Syst. 2011;33(3):472–6. https://doi.org/10.1016/j.ijepes.2010.10.010. http://www.sciencedirect.com/science/article/pii/S0142061510001973
[16] Sun F, Hu X, Zou Y, Li S. Adaptive unscented Kalman filtering for state of charge estimation of a lithium-ion battery for electric vehicles. Energy 2011;36(5):3531–40. https://doi.org/10.1016/j.energy.2011.03.059. http://www.sciencedirect.com/science/article/pii/S0360544211002271
[17] Walker E, Rayman S, White RE. Comparison of a particle filter and other state estimation methods for prognostics of lithium-ion batteries. J. Power Sources 2015;287:1–12. https://doi.org/10.1016/j.jpowsour.2015.04.020. http://www.sciencedirect.com/science/article/pii/S037877531500659X
[18] Orchard ME, Hevia-Koch P, Zhang B, Tang L. Risk measures for particle-filtering-based state-of-charge prognosis in lithium-ion batteries. IEEE Trans. Ind. Electron. 2013;60(11):5260–9. https://doi.org/10.1109/TIE.2012.2224079.
[19] Chang W-Y. The state of charge estimating methods for battery: a review. ISRN Appl. Math. 2013;2013. https://doi.org/10.1155/2013/953792.
[20] Goebel K, Saha B, Saxena A, Celaya J, Christophersen J. Prognostics in battery health management. Instrum. Measure. Mag. IEEE 2008;11(4):33–40. https://doi.org/10.1109/MIM.2008.4579269.
[21] Liu J, West M. Sequential Monte Carlo Methods in Practice. Springer New York; 2001. p. 197–223. Chapter: Combined Parameter and State Estimation in Simulation-Based Filtering
[22] Orchard ME, Vachtsevanos GJ. A particle-filtering approach for on-line fault diagnosis and failure prognosis. Trans. Inst. Measur. Control 2009;31(3/4):221–46. https://doi.org/10.1177/0142331208092026.
[23] Lughofer E, Pollak R, Zavoianu A-C, Pratama M, Meyer-Heye P, Zörrer H, et al. Self-adaptive evolving forecast models with incremental pls space updating for on-line prediction of micro-fluidic chip quality. Eng. Appl. Artif. Intell. 2018;68:131–51. https://doi.org/10.1016/j.engappai.2017.11.001. http://www.sciencedirect.com/science/article/pii/S0952197617302774
[24] Daigle M, Kulkarni C. Electrochemistry-based battery modeling for prognostics. 2013 International Conference on Prognostics and Health Management. 2013.
[25] Federal Aviation Administration. Helicopter Flying Handbook. Skyhorse Publishing9781620874929; 2013. Chapter: Helicopter Performance, https://books.google.cl/books?id=5QVECgAAQBAJ
[26] Daigle MJ, Goebel K. Model-based prognostics with concurrent damage progression processes. IEEE Trans. Syst. Man Cybern. 2013;43(3):535–46. https://doi.org/10.1109/TSMCA.2012.2207109.
[27] Daigle M.. Prognostics algorithm library [computer software]. https://www.github.com/nasa/PrognosticsAlgorithmLibrary; 2016a.
[28] Burgos-Mellado C, Orchard ME, Kazerani M, Cárdenas R, Sáez D. Particle-filtering-based estimation of maximum available power state in lithium-ion batteries. Appl. Energy 2016;161:349–63. https://doi.org/10.1016/j.apenergy.2015.09.092. http://www.sciencedirect.com/science/article/pii/S0306261915012180
[29] Tampier C, Pérez A, Jaramillo F, Quintero V, Orchard M, Silva J. Lithium-ion battery end-of-discharge time estimation and prognosis based on bayesian algorithms and outer feedback correction loops: a comparative analysis. Annual Conference of Prognostics and Health Management Society. PHM Society; 2015.
[30] Cisco Systems, Inc. Congestion avoidance overview, cisco IOS quality of service solutions configuration guide. http://www.cisco.com/c/en/us/td/docs/ios/12_2/qos/configuration/guide/fqos_c/qcfconav.html; 2014.
[31] Stepniewski WZ. Rotary-wing Aerodynamics. Volume I: Basic Theories of Rotor Aerodynamics with Application to Helicopters. vol. I. Washington, United States: National Aeronautics and Space Administration NASA, Scientific and Technical Information Office; 1979. p. 44–90. Chapter: Momentum Theory
[32] Engel SJ, Gilmartin BJ, Bongort K, Hess A. Prognostics, the real issues involved with predicting life remaining. 2000 IEEE Aerospace Conference. Proceedings (Cat. No.00TH8484). 6. 2000. p. 457–469vol.6. https://doi.org/10.1109/AERO.2000.877920.
[33] Saxena A, Celaya J, Balaban E, Goebel K, Saha B, Saha S, et al. Metrics for evaluating performance of prognostic techniques. 2008 International Conference on Prognostics and Health Management. 2008. p. 1–17. https://doi.org/10.1109/PHM.2008.4711436.
[34] Saxena A, Celaya J, Saha B, Saha S, Goebel K. On applying the prognostic performance metrics. 2009 International Conference on Prognostics and Health Management. 2009.
[35] Olivares BE, Munoz MAC, Orchard ME, Silva JF. Particle-filtering-based prognosis framework for energy storage devices with a statistical characterization of state-of-health regeneration phenomena. IEEE Transactions on Instrumentation and Measurement 2013;62(2):364–76. https://doi.org/10.1109/TIM.2012.2215142.
[36] Daigle M.. Prognostics model library [computer software]. https://www.github.com/nasa/PrognosticsModelLibrary; 2016b.